http://dx.doi.org/10.1039/c3sm52428k

Soft Matter

PAPER

Using AFM to probe the complexation of DNA with anionic lipids mediated by Ca^{2+}: the role of surface pressure†

Cite this: DOI: 10.1039/c3sm52428k

German Luque-Caballero, Alberto Martín-Molina, Alda Yadira Sánchez-Treviño, Miguel A. Rodriguez-Valverde, Miguel A. Cabrerizo-Vilchez and Julia Maldonado-Valderrama*

Complexation of DNA with lipids is currently being developed as an alternative to classical vectors based on viruses. Most of the research to date focuses on cationic lipids owing to their spontaneous complexation with DNA. Nonetheless, recent investigations have revealed that cationic lipids induce a large number of adverse effects on DNA delivery. Precisely, the lower cytotoxicity of anionic lipids accounts for their use as a promising alternative. However, the complexation of DNA with anionic lipids (mediated by cations) is still in early stages and is not yet well understood. In order to explore the molecular mechanisms underlying the complexation of anionic lipids and DNA we proposed a combined methodology based on the surface pressure–area isotherms, Gibbs elasticity and Atomic Force Microscopy (AFM). These techniques allow elucidation of the role of the surface pressure in the complexation and visualization of the interfacial aggregates for the first time. We demonstrate that the DNA complexes with negatively charged model monolayers (DPPC/DPPS 4 : 1) only in the presence of Ca^{2+}, but is expelled at very high surface pressures. Also, according to the Gibbs elasticity plot, the complexation of lipids and DNA implies a whole fluidisation of the monolayer and a completely different phase transition map in the presence of DNA and Ca^{2+}. AFM imaging allows identification for the first time of specific morphologies associated with different packing densities. At low surface coverage, a branched net like structure is observed whereas at high surface pressure fibers formed of interfacial aggregates appear. In summary, Ca^{2+} mediates the interaction between DNA and negatively charged lipids and also the conformation of the ternary system depends on the surface pressure. Such observations are important new generic features of the interaction between DNA and anionic lipids.

Received 15th September 2013
Accepted 10th January 2014

DOI: 10.1039/c3sm52428k

www.rsc.org/softmatter

1. Introduction

Lipoplexes are mesoscopic complexes that are produced by the complexation of the liposomes with nucleic acids (DNA or RNA). They are currently being developed for their use as non-viral vectors in gene therapy.[1–3] Usually, cationic lipoplexes made from positively charged liposomes are used, since they complex spontaneously with the DNA, which is negatively charged in solution.[4,5] These generally contain zwitterionic lipids in order to increase their transfection efficiency *in vitro*.[6–9] However, experimental studies have shown that cationic lipoplexes cause cytotoxicity, both *in vitro* and *in vivo*,[10,11] hence limiting their applicability. As a result, the complexation of anionic liposomes with DNA (anionic lipoplexes) is becoming an alternative to classical cationic lipoplexes due to their lower cytotoxicity. Furthermore, mixtures of zwitterionic and anionic naturally occurring phospholipids used to prepare anionic lipoplexes do not react with the serum proteins, thus enhancing transfection efficiency.[10,11] However, in contrast to cationic lipoplexes, the complexation of anionic liposomes with DNA is not spontaneous any more, but requires multivalent cations. As a result, the system now comprises an intricate electrostatic map in which the formation of anionic lipoplexes becomes a difficult task.[12]

To date, the optimization of the ratio of lipids, cations, and DNA has been addressed mainly phenomenologically by directly testing the transfection efficiency of the resulting lipoplexes.[13] However, basic physicochemical studies dealing specifically with the structure and morphology of anionic lipoplexes are still very scarce. For instance, Liang *et al.* investigated the structure and interactions of anionic lipoplexes in the presence of different divalent metal cations such as Mg^{2+}, Ca^{2+}, Co^{2+}, Cd^{2+}, Mn^{2+} and Zn^{2+} by performing SAXS experiments and confocal microscopy.[14] Therein, the type and concentration of the cation are determinants in the resulting transfection

Department of Applied Physics, University of Granada, Campus de Fuentenueva sn, 18071, Granada, Spain. E-mail: julia@ugr.es

† Electronic supplementary information (ESI) available. See DOI: 10.1039/c3sm52428k

efficiency[14,15] although the specific mechanisms involved still remain not completely understood. Therefore, advances in this field require a detailed characterization of their structure and their function in all the stages during the transfection process, from the cell uptake to the gene delivery inside the cell. In the case of cationic lipoplexes, the resulting structures are experimentally studied by cryo-electron microscopy (Cryo-TEM) and small-angle X-ray scattering (SAXS).[6–8,16] Although the preparation of the samples is very different in both techniques, a satisfactory agreement can be reached in the results obtained from them.[6,8] However, quantitative approaches to structural relationships of anionic lipoplexes are challenging due to the multitude of components which makes difficult to study them *in situ*.

Therefore, there is a great need for simplified model systems to get direct relationships between the microscopic properties and the macroscopic observables. The use of physicochemical tools as a probe of molecular interactions in monolayers is already longstanding. Moreover, surface interactions between the polar headgroups of lipids and cations play a role in the formation of anionic lipoplexes by promoting interfacial adsorption phenomena. For instance, Ohki and Düzgunes demonstrated that the water-exclusion effect caused by the formation of a cation/lipid complex in the monolayer was essential for the liposome–monolayer membrane fusion process.[17] More recently, light scattering experiments have proved that similar divalent cations such as Ca^{2+} and Mg^{2+} induce different structural changes in anionic phospholipid membranes and different membrane solvations, which in turn has substantial consequences in the interaction between membranes and their aggregation behaviour.[18–20] Also, Wangerek *et al.* have monitored the DNA compaction degree for different types of cationic lipoplexes by dynamic light scattering (DLS) and AFM.[21] They analysed the implications of these results on transfection efficiency using *in vitro* experiments: immortalized cells showed optimal transfection efficiency with multivalent lipids, which gave compact structures, while primary neurons showed optimal transfection with monovalent lipids, which gave less compact structures. Marty *et al.* also investigated the structure of cationic and zwitterionic lipoplexes with AFM, describing aggregates with a core and a more deformable lipid shell for DOTAP (1,2-dioleoyl-3-trimethylammonium-propane)/DNA cationic lipoplexes.[22] Kim *et al.* showed that malachite green displayed different orientations during the interfacial adsorption on a dipalmitoylphosphatidylglycerol (DPPG) negatively charged monolayer depending on the phase organization of the monolayer.[23]

In fact, Langmuir monolayers in combination with other experimental techniques have been used to characterize the lipid–DNA interaction in order to understand and improve cationic and zwitterionic lipoplexes.[24–29] Nevertheless, the interaction between anionic lipid monolayers and DNA mediated by multivalent cations has been much less studied. Frantescu *et al.* reported the characterization of a negatively charged lipid monolayer on a subphase containing both DNA and divalent cations.[30] Therein, adsorption of DNA on plasma cell membranes for DNA electrotransfer purposes was studied, unfortunately implications with anionic lipoplexes were not described. In this sense, the air–water interface represents an ideal fluid support for surface organization at interfaces, thus being susceptible to thermodynamic and structural characterization. In particular, lipid monolayers show a well-defined surface pressure, π, quantified as the free energy gained upon molecular adsorption at a given surface concentration. Once spread, lipid molecules can be laterally compressed under the action of the barriers of the Langmuir trough, thus allowing accessible different packing states. Accordingly, Langmuir lipid monolayers constitute a suitable methodological approach for characterizing the physicochemical properties of lipoplexes by addressing the interaction of DNA with lipids at the air–water interface. Moreover, Langmuir–Blodgett (LB) transfer of these films provides a solid support for applying Scanning Probe Microscopy Tools.[31]

Once again, this technique has been applied for imaging positively charged amphiphile monolayers at the air–DNA solution interface.[32–34] Much less studied is the case of anionic monolayers with the exception of Dubrovin *et al.* who reported that polyadenylic acid (poly(A)) interfacial adsorption on stearic acid monolayers, with negative surface charge density, took place in the presence of Na^+ or Mg^{2+} cations. They used the LB-AFM technique to monitor the increase in the number of poly(A) fibers attached to the stearic acid monolayer as a function of increasing concentrations of NaCl. Since they observed no poly(A) adsorption in the presence of both 1 M NaCl and the chelating agent ethylenediaminetetraacetic acid (EDTA) at the concentration of 10 mM, they concluded that the divalent cations, which are present as minor components in the monovalent salts, were essential to bridge the interaction between the stearic acid monolayer and the poly(A).[35]

Accordingly, our goal here is to use a model system to study the fundamentals and the basis of the complexation of DNA with anionic lipids at interfaces mediated by Ca^{2+} as influenced by lateral packing. As anionic substrates we used a mixture of phospholipids, DPPC (zwitterionic) and DPPS (anionic), in a molar ratio 4 : 1; this monolayer has been previously characterized at the air–water interface.[36] Then, we used the LB-AFM technique to visualize the system. The combined use of surface pressure and AFM-imaging appears as a novel strategy to improve the understanding of the interactions between the different molecules involved in the formation of anionic lipoplexes. We believe that scientific advances in the interfacial properties of such model ternary systems will assist in the rational design and development of low toxicity, non-viral gene vectors.

2. Experimental section

2.1. Materials

Phospholipids, dipalmitoylphosphatidylcholine (DPPC) and dipalmitoylphosphatidylserine (DPPS), were purchased from Sigma (>99% purity) and used as supplied. Solutions of 0.5 mg ml^{-1} DPPC/DPPS 4 : 1 (mol mol^{-1}) mixtures were prepared by dissolving the phospholipids in chloroform/methanol 4 : 1 (v/v) under ambient conditions. These spreading solvents were of

analytical grade (Scharlau) and used as received. Double stranded DNA from calf thymus was purchased from Sigma (>98% purity). The purity of the DNA was tested by measuring the absorbance at 260 and 280 nm providing values of $A_{260}/A_{280} \approx 1.8$ which confirmed negligible protein contamination in the sample. In order to reduce the mean size of the DNA provided, it was fragmented before use by adapting the procedure described elsewhere.[28,37,38] A stock solution of 4 mg ml^{-1} DNA was prepared by mixing the DNA solid fibers with water and stored at 4 °C without any agitation for 3 days. This solution was then sonicated in a sonication bath for 10 h under a N_2 stream to prevent oxygen degradation. The size of the fragmented DNA was tested by agarose gel electrophoresis of the sonicated solution which provided a size distribution ranging between 300 and 1300 base pairs, hence assuring the fragmentation of the DNA. These fragmented DNA solutions were stored at −20 °C until their use. $CaCl_2 \cdot 2H_2O$ was purchased from Sigma (>99% purity) and used as supplied.

Ultrapure water purified by a Milli-Q plus water purification system (resistivity 18.2 MΩ cm) was used for the preparation of solutions. All glassware was cleaned with 10% Micro-90® cleaning solution, isopropanol and then repeatedly rinsed with distilled and ultrapure water.

2.2. Langmuir monolayers

Phospholipid monolayers at the air–water interface were formed in a Langmuir trough of total area 244.5 cm^2, equipped with paper Wilhelmy plates pressure measuring system (KSV) with a π sensitivity of 0.1 mN m^{-1}. The trough was first cleaned with 10% Micro-90® cleaning solution, isopropanol and then repeatedly rinsed with distilled and ultrapure water and the absence of surface active contaminants was verified by compressing the bare water subphase, obtaining values of $\pi < 0.2$ mN m^{-1} within the whole compression cycle. Then, 50 ml of phospholipid solution (0.5 mg ml^{-1} DPPC/DPPS 4 : 1 (mol/mol)) were carefully spread on the subphase by means of a microsyringe (Hamilton®). After an evaporation time of 20 min, the surface pressure–area (π–A) is recorded upon symmetric uniaxial compression at a constant rate of 3.75 cm^2 min^{-1}. First, the π–A isotherm of the DPPC/DPPS 4 : 1 was measured on pure water. Then, the experiment is repeated using a 5 mM $CaCl_2$ solution as a subphase and, later on, with a 0.1 mg ml^{-1} DNA solution. Finally, the effect of DNA and Ca^{2+} together was tested by spreading the DPPC/DPPS 4 : 1 on a subphase containing both 5 mM $CaCl_2$ and 0.1 mg ml^{-1} DNA at the same time, and recording the π–area isotherm. The whole experiment series (DPPC/DPPS 4 : 1 monolayer spread on water, Ca^{2+}, DNA and Ca^{2+} + DNA subphase) were carried out on the same day with the same phospholipid solution in order to keep constant all the conditions. The reproducibility of the π-area isotherms of the DPPC/DPPS 4 : 1 monolayer spread on water or on a Ca^{2+} + DNA subphase was tested by independent measurements carried out in triplicate for independent samples. The whole setup was located in a transparent Plexiglas case to avoid air streams and dust deposition and to allow temperature control at 20.0 ± 0.1 °C.

The surface Gibbs elasticity[39] of the monolayer was calculated directly from the π–A isotherms using eqn (1):

$$\varepsilon_0 = -A\left(\frac{\partial \pi}{\partial A}\right)_T \quad (1)$$

where π is the surface pressure of the monolayer and A is the area of the monolayer.

2.3. Atomic Force Microscopy

Surface films were sampled by transferring materials onto freshly cleaved mica (Agar Scientific) using the Langmuir–Blodgett (LB) technique at various selected surface pressures, as described elsewhere.[40] LB films were prepared by vertical dipping into the subphase at a constant surface pressure. This is automatically done by KSV-LB software. The mica support was first immersed and then extracted from the subphase. The transfer rate was 5 mm min^{-1} for the monolayers prepared on either pure water or DNA subphases and 2 mm min^{-1} for the monolayers prepared on a subphase containing DNA and $CaCl_2$. In this way, transfer ratios were 0 during the immersion while they were 1 for the extraction process, proving the film deposition at this stage. The samples collected were allowed to dry before imaging. Imaging of transferred Langmuir–Blodgett films was carried out using an Atomic Force Microscope Nanoscope IV MultiMode in air (Digital Instruments, Santa Barbara, Ca, USA). Images were obtained in tapping mode with a Si-doped P(u) cantilever. The topography data were sampled in a grid of 512 × 512 points or 1024 × 1024 points. The imaging was carried out under ambient laboratory conditions. The structures seen following LB transfer of phospholipids correspond with those present at the air–water interface as has been demonstrated using Brewster Angle Microscopy (BAM).[40] Each sample was imaged in at least two different areas obtaining similar patterns. The reproducibility of the current experiments was tested by measurements in duplicate for the DPPC/DPPS 4 : 1 monolayers spread on pure water at 2 mN m^{-1} and on a Ca^{2+} + DNA subphase at 25 and 40 mN m^{-1}, obtaining similar patterns. AFM images were processed with open source software Gwyddion 2.22 (http://www.gwyddion.net), which was used also to determine height distribution functions.

3. Results and discussion

3.1. π–A isotherm of the phospholipid/Ca^{2+}/DNA monolayer

Fig. 1 shows the π–A isotherms (surface pressure *versus* mean molecular area) obtained for DPPC/DPPS 4 : 1 spread on water, on Ca^{2+}, on DNA and on Ca^{2+} + DNA subphases. The mean molecular area per lipid molecule is obtained by dividing the surface area available between the barriers by the total amount of spread phospholipids. It can be seen that the isotherm remains invariable under the presence of Ca^{2+} alone while it is affected by the presence of DNA, alone or in combination with Ca^{2+}, the effect being stronger when both components are present together in the subphase. Let us discuss these isotherms (Fig. 1) in more detail.

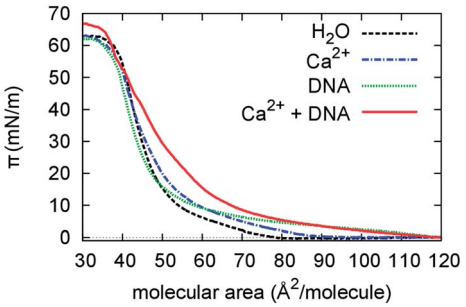

Fig. 1 π-area isotherms of a DPPC/DPPS 4:1 monolayer spread on different subphases: (a) pure water (black dashed line), (b) 5 mM $CaCl_2$ (blue dash-dotted line), (c) 0.1 mg ml^{-1} DNA (green dotted line) and (d) 5 mM $CaCl_2$ and 0.1 mg ml^{-1} DNA (red line). $T = 20$ °C.

First, the π–A isotherm of DPPC/DPPS 4 : 1 spread on water displays an irregular increase in surface pressure showing a number of distinct regions upon lateral compression (Fig. 1). Following the general assignments for the phospholipid phases in the literature,[41] these regions were assigned as gas–LE (liquid expanded), LE, LE–LC (liquid condensed), LC and collapse phases. The surface pressure lifted off at 90 ± 8 Å^2 per molecule (mean value of three measurements) and entered a linear regime lasting until approximately 6.2 ± 0.6 mN m^{-1} when the isotherm exhibits a transition region for $6 < \pi < 10$ mN m^{-1}, implying the coexistence of LE and LC phases. Further compression led to a LC phase characterized by a very steep increase of the surface pressure, and finally the isotherm reached a collapse pressure of 55 ± 1 mN m^{-1} (mean value of three measurements). The shapes of the isotherms in Fig. 1 are in good correlation with the π–A isotherm reported by Ross *et al.*[36] for the same lipid mixture.

Before addressing the combined effect of the Ca^{2+} cations and DNA at the same time, the effect of these substances on the monolayer was characterized separately. The π–A isotherms of the DPPC/DPPS 4 : 1 spread on either 5 mM $CaCl_2$ or 0.1 mg ml^{-1} DNA are also plotted in Fig. 1. No significant changes with respect to the isotherm recorded on pure water were observed for $CaCl_2$ and the slight differences between both isotherms are smaller than the experimental error. Furthermore, our findings confirm those reported by Ross *et al.*[36] who also show that the shape of the isotherm was unaffected by the presence of Ca^{2+} in the subphase. However, when a 0.1 mg ml^{-1} DNA solution was used as the subphase, the isotherm is shifted to slightly higher molecular areas with the lift off at the beginning of the compression (Fig. 1). The displacement to higher molecular areas remains for the linear region and the first part of the LE–LC transition region but disappears at higher compression, overlapping with the isotherm recorded on pure water for surface pressures above 15 mN m^{-1}.

Conversely, the isotherm recorded for DPPC/DPPS 4 : 1 spread on a subphase containing DNA and Ca^{2+} displays significant differences with respect to the one spread on pure water (Fig. 1). Firstly, the surface pressure starts to increase almost from the beginning of the compression. This already suggests the higher separation of the polar heads of the phospholipids at the surface. Secondly, the whole curve is displaced to higher molecular areas, not only at low surface pressures, but also at high surface pressures corresponding to the LC region. Also, the well defined LE–LC coexistence region ($6 < \pi < 10$ mN m^{-1}) is less clear in the case of DNA and Ca^{2+}. Instead, the surface pressure increases smoothly suggesting the existence of a pseudo liquid-expanded (LE) phase from the gas–LE coexistence or else a large LE–LC coexistence phase. Finally, at a surface pressure of 46 ± 7 mN m^{-1}, the slope changes abruptly and the isotherm overlaps with that recorded on a pure water subphase until collapse. The differences encountered in each of these separated regions are discussed in detail below.

Firstly, concerning the earlier lift off of the isotherm recorded in the presence of Ca^{2+} and DNA, the surface pressure starts to increase linearly from the very beginning of the compression for the Ca^{2+} + DNA subphase. This enhanced compression sensitivity of the monolayer was also observed for the DNA subphase without Ca^{2+} (Fig. 1), so it cannot be related solely to the presence of cations. Ross *et al.*[36] also observed a remarkable increase in the molecular area corresponding to the π lift off with the same monolayer and using as a subphase a solution containing EGTA (ethylene glycol-bis(β-aminoethyl) ether-*N*,*N*,*N*′,*N*″-tetraacetic acid). They showed that, as a result of the EGTA cation removal, the miscibility of the two lipids increased, producing an increase in the total packing density. Since DNA is a negatively charged polyelectrolyte, it may produce a similar effect as the EGTA.

Secondly, regarding the shift to higher molecular areas, we can distinguish three regions in the isotherm recorded in the presence of Ca^{2+} and DNA. At low surface pressures the isotherm overlaps with the one recorded in the presence of DNA without Ca^{2+}. The displacement to higher molecular areas remains during the whole LE–LC region until very high compression states where the isotherm overlaps with that recorded on pure water. Accordingly, the net expansion of the isotherm reveals that the average intermolecular distance between polar heads increases due to the migration of the DNA into the monolayer. This can be explained in terms of Ca^{2+} playing the role of a bridge between the negatively charged phospholipid monolayer and the DNA, leading to the formation of a monolayer/Ca^{2+}/DNA complex. This effect has been recorded so far only for zwitterionic monolayers, which lack a net charge. Hence, Gromelski and Brezesinski prove the penetration of DNA into a DMPE monolayer by recording a shift to higher molecular areas of DMPE in the presence of DNA and Mg^{2+} cations.[42] Similarly, according to McLoughlin *et al.*,[28] the Ca^{2+} is able to induce this sort of shift to higher molecular areas in a π–A isotherm for a zwitterionic monolayer (DPPC) in the presence of DNA. Concerning the behaviour of the zwitterionic monolayer/cation/DNA ternary complex, Mengistu *et al.* developed a theoretical approach based on the classical Poisson Boltzmann formalism to look into the role of divalent cations in the formation of this type of ternary complex.[43] Therein, the authors report that the DNA adsorption process is accompanied by a redistribution of divalent cations from the DNA to the anionic moieties in the lipid headgroups, indicating that the

DNA-induced cation penetration into the headgroup region resulted in a lateral condensation in the monolayer.

Accordingly, Fig. 1 demonstrates for the first time the penetration of DNA into an anionic lipid monolayer of DPPC/DPPS mediated by Ca^{2+}. Additionally, we may quantify the shift in molecular area units in Table 1 obtaining similar values for the pure DPPC and the mixture DPPC/DPPS 4 : 1. Accordingly, the effect observed in the π–A isotherm appears mainly surface charge-independent. This finding should be taken into account in order to understand the molecular mechanism underlying this interaction, which cannot be understood by pure electrostatic effects.

Finally, the overlap of the two isotherms seen at very high surface pressures (π > 52 mN m^{-1}) possibly implies that the DNA is being squeezed out of the monolayer at very high lateral packing. This sort of surface pressure-induced DNA detachment has so far only been reported for pure zwitterionic lipids[42,44] since, Frantescu *et al.*[30] do not find this overlapping tendency for POPC/PS 2 : 1/Ca^{2+}/DNA. This apparent controversy could originate in the nature of the lipid monolayer, rather than in the net charge. The collapse of unsaturated phospholipids is reached at significantly lower surface pressures than the saturated ones. Accordingly, the detachment of DNA from the former case is not observed because the steric instability induced by the double bonds provokes the collapse of the monolayer before reaching a sufficiently high surface pressure to squeeze out the DNA. Hence, unsaturated lipid monolayers are not sufficiently condensed to squeeze out the DNA. This is a very important finding that must be considered when designing lipoplexes with different anionic lipids.

3.2. Surface Gibbs elasticity

Fig. 1 shows experimental evidence about structural changes induced by DNA in phospholipid monolayers in the presence of Ca^{2+}. To gain further structural insights into the conformation of the system we now look into the Gibbs elasticity of the monolayers, a property sensitive to molecular conformation. Fig. 2 shows the Gibbs elasticity plot of the isotherms of DPPC/DPPS 4 : 1 monolayers spread on water or on a subphase containing DNA and Ca^{2+} from Fig. 1. Given that only the π–A isotherm of the DPPC/DPPS 4 : 1/Ca^{2+}/DNA has shown significant differences from the pure DPPC/DPPS 4 : 1 system, we only compare these two systems in Fig. 2. Gibbs elasticity (ε_0) is an elastic modulus representing a rheological quantity related to the monolayer rigidity and to its capability to store elastic energy, which is defined by eqn (1). The compression of the monolayer is performed at a sufficiently low rate to ensure that the system is always in a stationary state and possible relaxation processes in the monolayer can be neglected. Hence, at this compression rate and for insoluble monolayers, the Gibbs elasticity plotted in Fig. 2 provides generic information on the mechanical state of the monolayer.

Table 1 π-area isotherm shift (ΔA) at different surface pressures for DPPC and DPPC/DPPS 4 : 1 Langmuir monolayers on a subphase containing 5 mM $CaCl_2$ and 0.1 mg ml^{-1} DNA with respect to the same monolayer on pure water

	ΔA (Å^2 per molecule)	
π (mN m^{-1})	DPPC	DPPC/DPPS 4 : 1
10.0 ± 0.1	9 ± 5	12 ± 3
20.0 ± 0.1	6 ± 4	8.5 ± 2.2
30.0 ± 0.1	3.3 ± 2.3	4.2 ± 1.7
40.0 ± 0.1	1.5 ± 1.5	1.3 ± 1.5

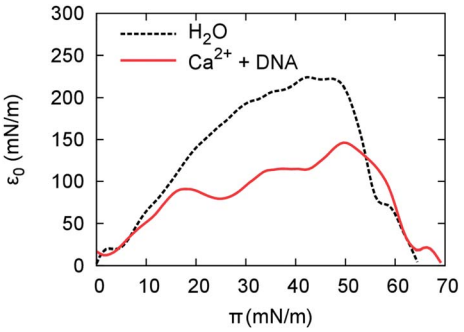

Fig. 2 ε_0–π plots from (a) and (d) curves in Fig. 1. DPPC/DPPS 4 : 1 monolayer spread on: pure water subphase (black dashed line), 5 mM $CaCl_2$ and 0.1 mg ml^{-1} DNA subphase (red line). T = 20 °C.

In general, ε_0 increases upon lateral compression meaning that the higher the phospholipid packing density, the higher the resistance of the monolayer to deformation. However, this general tendency is altered by any phase transition event. The coexistence of different phases leads to a local minimum of ε_0 owing to a decreasing cohesion of the surface film, which is disrupted by the presence of the new phase.[45] The Gibbs elasticity increases again as the surface layer fills with the new phase and reaches a maximum at the maximum packing density in the new phase. A new transition within the monolayer would imply a new local decrease. Accordingly, the minima reflect phase coexistences in the monolayer whereas the maxima in the Gibbs elasticity plot are ascribed to the existence of a homogeneous cohesive layer.

For the DPPC/DPPS 4 : 1 spread on a pure water subphase (Fig. 2), we can distinguish two ε_0 local maxima located at $\pi = 3 \pm 1$ and $\pi = 44 \pm 2$ mN m^{-1} (mean values of three measurements). The first corresponds to the elasticity of a monolayer in the LE state ($\varepsilon_0 = 22 \pm 3$ mN m^{-1}) followed by the LE–LC transition in which the ε_0 decreases locally to a minimum. The second maximum corresponds to the elasticity of the monolayer in the LC state ($\varepsilon_0 = 239 \pm 17$ mN m^{-1}) followed by collapse of the monolayer (mean values of three measurements). Clearly, the rigidity of the monolayer is substantially higher at the LC state. After the second maximum, the ε_0 drops sharply indicating that the monolayer has broken down, with the formation of a variety of bidimensional and tridimensional structures.

The evolution of ε_0 as a function of lateral packing changes in the presence of both Ca^{2+} and DNA in the subphase. In general, it appears to be significantly lower than the values corresponding to the pure water subphase. This means that the monolayer formed on the subphase containing both Ca^{2+} and

DNA is more deformable than that recorded on a pure water subphase. Structural differences between the DPPC/DPPS 4 : 1 and DPPC/DPPS 4 : 1/Ca^{2+}/DNA systems were already inferred from Fig. 1 at these surface pressures. We denoted this region (π < 52 mN m^{-1}) as the pseudo liquid-expanded (LE) or long LE–LC coexistence phase in the previous section. Interestingly, Jain *et al.*[46] reported a similar decrease in the dilational elasticity modulus as a consequence of the binding of the polyacrylamide sulfonate polyanion to a cetyltrimethylammonium bromide monolayer. Hence, the lower elasticity could indicate binding of the DNA to the DPPC/DPPS assisted by Ca^{2+} which results in the fluidisation of the surface film.

At higher surface pressures (π > 52 mN m^{-1}) the ε_0-π curve for the DPPC/DPPS 4 : 1/Ca^{2+}/DNA system displays a sharp increase and a last maximum which precedes collapse. The elasticity of the mixture in this last region is clearly higher and approaches that of the phospholipid mixture on pure water. Accordingly, the DNA is being expelled from the monolayer and the cohesion increases as the non-complexed monolayer is restored.

We can also appreciate a new local maximum–minimum distribution in the ε_0-π curve for the DPPC/DPPS 4 : 1/Ca^{2+}/DNA system. This certainly shows that the formation of the monolayer/Ca^{2+}/DNA complex is accompanied by a totally different phase rearrangement from that on water. The minima located at 2, 25 and 40 mN m^{-1} in Fig. 2 were selected for LB-AFM examination with the aim of visualizing the morphology of the coexisting phases in the monolayer/Ca^{2+}/DNA complex.

3.3. Imaging with AFM

In order to further analyze the origins of the observed changes in surface tension and Gibbs elasticity, we have imaged the changes in the morphology of the DPPC/DPPS 4 : 1/Ca^{2+}/DNA system by means of Atomic Force Microscopy (AFM). In this way, we assess the effect of Ca^{2+} and DNA on the structure of DPPC/DPPS 4 : 1 monolayers by following a similar experimental procedure to that of the previous sections. Hence, we analyze first the separate effect of Ca^{2+} and DNA on the DPPC/DPPS 4 : 1 monolayer and then examine the ternary system. Images were taken in tapping mode so that differences in contrast are caused by a difference in the tip–surface interaction which is ascribed to the local topography, roughness, adhesion or elasticity in each sort of domain. The AFM images have been further analyzed in order to quantify the different morphologies encountered. Table 2 displays a summary of the various systems analyzed including a description of the basic appearance of each system, identification of the different morphologies, the Root Mean Square Roughness (RMS) and the height distribution as an average of all the images.

Consider first the DPPC/DPPS 4 : 1 spread on a pure water subphase (Fig. 3A). In order to visualize morphological aspects we chose a surface pressure of 2 mN m^{-1} where we have LE and LC phase coexistence according to the surface pressure isotherms (Fig. 1) and Gibbs elasticity (Fig. 2) as discussed above. Fig. 3 reveals the existence of LE and LC phase coexistence as given by a background (LE) spotted by round-shaped domains (LC). The existence of these domains has been also reported by Ross *et al.* for the same lipid mixture and attributed to lipid demixing and the formation of DPPS-enriched domains.[36] The LE–LC coexistence phase for DPPC takes place above 4 mN m^{-1} whereas DPPS is in the LC state at π = 2 mN m^{-1} (see ESI, Fig. S1†). In the mixed system, LC domains are present from the beginning of the compression and possibly act as nucleation sites. The mixed system continuously undergoes LE–LC phase transition even at surface pressures well below 4 mN m^{-1} leading to a continuous growth of the circular domains as the surface pressure increases (Fig. 3). Accordingly, the circular domains in Fig. 3 correspond to DPPS enriched areas. At this surface coverage the round-shaped domains have a diameter of 4 ± 3 μm and the relative domain surface coverage is 72 ± 4% (Fig. 3A). The diameter of these domains increases in size as the surface coverage is increased, hence indicating the transition to a LC phase (images not shown). Moreover, a very similar morphology was obtained for the AFM images of the DPPC/DPPS 4 : 1/Ca^{2+} binary system.

Fig. 3B shows also the AFM image of the DPPC/DPPS 4 : 1/DNA binary system at the same surface pressure (2 mN m^{-1}).

Table 2 Quantitative analysis of LB-AFM images

Subphase	π (mN m^{-1})	Morphology[a]	RMS[b] (nm)	Height distribution[c]
H_2O	2.0 ± 0.1	Round-shaped domains	0.3 ± 0.3	—
0.1 mg ml^{-1} DNA	2.0 ± 0.1	Round-shaped domains	0.4 ± 0.1	—
0.1 mg ml^{-1} DNA + 5 mM $CaCl_2$	2.0 ± 0.1	(a) Branched (b) Net-like	2.1 ± 0.4	—
0.1 mg ml^{-1} DNA + 5 mM $CaCl_2$	25.0 ± 0.1	(a) Granular (b) Holes and fibers	—	(b) Trimodal, Δh_1 = 1.59 ± 0.24 nm, Δh_2 = 1.1 ± 0.4 nm
0.1 mg ml^{-1} DNA + 5 mM $CaCl_2$	40.0 ± 0.1	(a) Elevations (b) Holes and fibers	—	(b) Trimodal, Δh_1 = 1.64 ± 0.23 nm, Δh_2 = 1.2 ± 0.4 nm

[a] When two different mesostructures coexist on the phospholipid/Ca^{2+}/DNA complex film they are separately described as (a) and (b). [b] The root mean square roughness is calculated to show the contrast between the LB phospholipid monolayer on pure water or on a DNA subphase with respect to the phospholipid/Ca^{2+}/DNA complex film. RMS is not calculated at 25 or 40 mN m^{-1} because the value would not be representative of the two different mesostructures in contact. [c] Height distribution functions. Height differences between the consecutive peaks are shown for bimodal and trimodal distributions. These height differences allow better characterization of (1) the LC domain height for a LB phospholipid monolayer prepared from a Langmuir monolayer on a subphase containing 0.1 mg ml^{-1} DNA (Δh) and (2) the depth of holes and the height of fibers (Δh_1 and Δh_2, respectively) in the background observed in the phospholipid/Ca^{2+}/DNA complex films at high surface pressures.

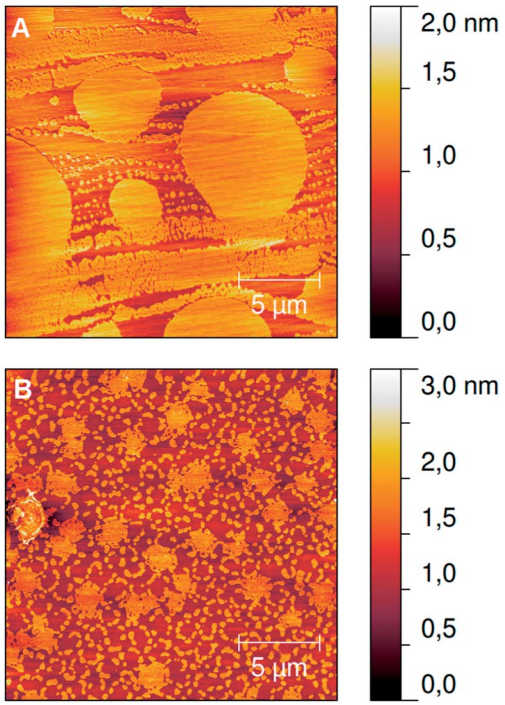

Fig. 3 AFM topography images of LB transferred DPPC/DPPS 4 : 1 spread on a pure water subphase (A) and 0.1 mg ml^{-1} ctDNA (B) at π = 2 mN m^{-1}. In both cases, surface films are heterogeneous showing regions with variable heights and circular domains.

Fig. 3B reveals again the existence of LE and LC phase coexistence as given by a background (LE) spotted by round-shaped domains (LC), which should again correspond to DPPS-enriched domains caused by demixing. However, the diameter of such domains seems to be reduced by the presence of DNA in the subphase obtaining now 1.4 ± 0.4 μm. The domain surface coverage is also reduced to 45 ± 3% suggesting that the demixing process is hindered by the presence of DNA in the subphase. According to Ross *et al.* the formation of DPPS enriched domains in Fig. 3A occurs owing to traces of Ca^{2+} present in water which are essential for the lipid demixing process as measured by TOF-SIMS.[36] In Fig. 3B, the DNA is likely to complex with the traces of Ca^{2+} in solution, hence playing a purifier role and lowering the residual concentration of Ca^{2+} in pure water, thus hindering the formation of DPPS-enriched domains. This interpretation is in good agreement with the π lift off at the beginning of compression observed in the π–*A* isotherm for this binary system (DPPC/DPPS 4 : 1/DNA) in Fig. 1. Moreover, this effect was also observed by Ross *et al.*[36] for the DPPC/DPPS 4 : 1/EGTA system and ascribed to the release of DPPS from the more condensed domains to the mixed monolayer. To sum up, the morphology of the DPPC/DPPS 4 : 1 monolayer spread on a subphase containing 0.1 mg ml^{-1} of DNA resembles the monolayer spread on pure water providing no evidence of the DNA complexation in the Langmuir–Blodgett transfer process in the absence of Ca^{2+}.

Before continuing the analysis of the AFM images and in order to improve the understanding of the results, it is important to discuss in depth the possible molecular mechanisms underlying the formation of these ternary complexes. Our results agree with those obtained by Ross *et al.* who already proved that Ca^{2+} preferentially binds to negatively charged DPPS molecules while a hydrated calcium–DPPS complex of larger dimensions is formed.[36] For the case of pure anionic lipid membranes it is also established experimentally that the binding of multivalent cations to negatively charged lipids is endothermic, and thus, entropically driven. This fact strongly suggests that the driving forces for ion binding are due to hydration and solvation effects as well as structural rearrangements in the membrane. Similarly, Sinn *et al.* reported that the presence of anionic phospholipids increased the interaction with Ca^{2+} and Mg^{2+} (ref. 47) but they showed by means of calorimetric measurements that the driving force of this interaction is the release of water molecules due to the dehydration of the cations and the phosphate groups, which is an entropically favorable process. Concerning the cation binding, early infrared spectroscopic studies demonstrate the formation of a strong Ca^{2+}-PO_4^- complex.[48] However, Boettcher *et al.* performed a combination of atomistic simulations with magic angle spinning (MAS) and solid-state NMR measurements to verify the binding of Ca^{2+} to carboxyl in the PS headgroup. Furthermore, all-atomistic simulations were used in ref. 20 and 49 to demonstrate that multivalent ions such as La^{2+}, Mg^{2+} and Ca^{2+} ions are incorporated deeply in the hydrophilic region of the PS membrane. In particular, adsorbed Ca^{2+} cations tend to be bound to 2 PS^- headgroups in a binding mode which involves both the carboxylic and phosphate moieties of the lipid headgroup. Accordingly, adsorption of Ca^{2+} cations on PS lipid membranes generates a highly inhomogeneous surface with patches of positive charge (both from lipids and ions) directed towards the aqueous phase that induce DNA adsorption *via* hydrogen bonding between the phosphate groups of DNA and the amino groups of PS (see ref. 12 and 50).

Fig. 4 shows the AFM images of the DPPC/DPPS 4 : 1/Ca^{2+}/DNA ternary system at 2 mN m^{-1}. Clearly, now totally different patterns appear in the monolayer, as compared with the pure lipid and the binary systems, with branched and net-like structures (Fig. 4). Also, the roughness of the monolayer spread on DNA and Ca^{2+} increases significantly with respect to that spread on DNA without Ca^{2+} as demonstrated by the higher value obtained for the RMS given in Table 2. Control AFM images of the DNA adsorbed on mica after LB deposition confirm that the phospholipid monolayer modulates the organization and morphology of the interfacial aggregates (see ESI, Fig. S2†). Thus, in view of the images and the RMS values, we can conclude that the lipid/Ca^{2+}/DNA ternary system forms interfacial aggregates dispersed on the film. A more detailed analysis of the pattern obtained in Fig. 4 allows distinguishing two different morphologies: round-shaped areas containing fractal branched structures with an average height of 8 nm (marked with + in Fig. 4A) and a background (marked with * in Fig. 4A). Moreover, the high resolution image in Fig. 4B allows further identification of a net of fibrils with an average height of 3 nm and width of 0.2 μm in the background. In fact, these fibrillar structures possibly correspond to interfacial aggregates formed as a result of the interaction among the phospholipids,

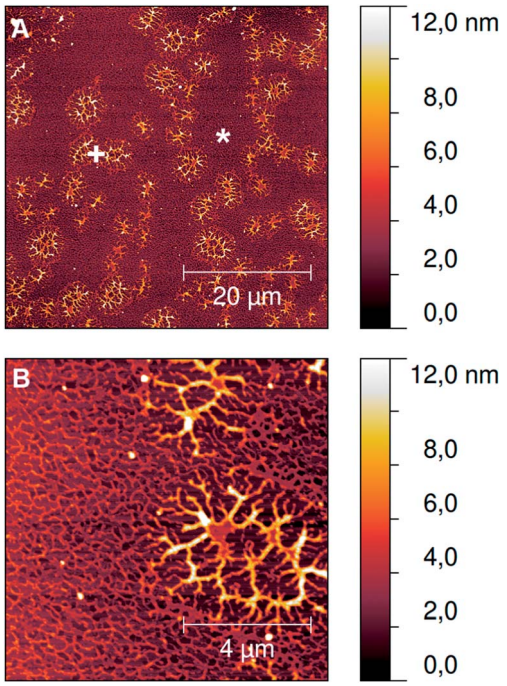

Fig. 4 (A) AFM topography image of LB transferred DPPC/DPPS 4 : 1 spread on an aqueous solution subphase containing 5 mM $CaCl_2$ and 0.1 ctmg ml^{-1} DNA at $\pi = 2$ mN m^{-1}. (B) High resolution image. The surface film reveals round-shaped areas containing fractal branched structures (+) and a background (*). The high-resolution image shows a surface network formed by fibrils.

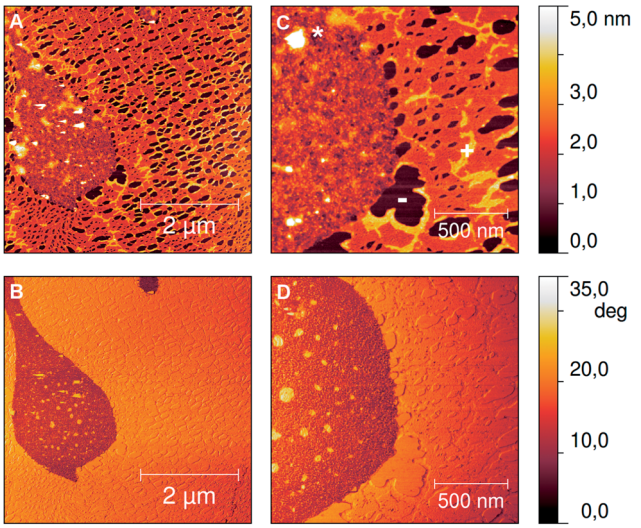

Fig. 5 AFM topography image of LB transferred DPPC/DPPS 4 : 1 spread on an aqueous solution subphase containing 5 mM $CaCl_2$ and 0.1 ctmg ml^{-1} DNA at $\pi = 25$ mN m^{-1}. (A) Height image, (B) phase image, (C) high resolution image, (D) phase from (C). Surface film shows circular domains with granular structure (*). The high-resolution image (C and D) reveals a background composed of a discontinuous plane with holes (–) and fibers (+).

the Ca^{2+} cations and the DNA. Similar patterns have been previously observed for other systems containing DNA; namely, by Chen *et al.*[33] for the gemini surfactant 18-*s*-18/DNA system and by Antipina *et al.*[32] for poly-4-vinylpyridine with 16% cetylpyridinium groups (PVP-16)/DNA. However, they have not been reported so far for lipids. The round-shaped areas with larger, branched fibrils are possibly composed of DPPS-enriched domains of the monolayer. DPPS, having higher surface charge density, leads to the complexation of a relatively higher amount of DNA with respect to the background (DPPC) and hence, the formation of bigger interfacial aggregates.

We analyze further the complexity of the interfacial structures of the DPPC/DPPS 4 : 1/Ca^{2+}/DNA ternary system at higher surface coverage (higher surface pressures). Fig. 5 shows the AFM-images recorded from LB films of the ternary system at 25 mN m^{-1}. In this case we can also identify two different sorts of domains which can be appreciated, both in the topographic (Fig. 5A and C) and in the phase (Fig. 5B and D) images. However, the shape and the fine structure of these domains are completely different from those seen at lower surface coverage: 2 mN m^{-1} (Fig. 4). On the one hand, we observe a curved domain with a granular structure (marked with * in Fig. 5C). These grains have an average diameter of 20 nm. On the other hand, the background presents structures with three well-defined different height levels. There is a discontinuous plane in which holes (depressions, – in Fig. 5C) and fibers (elevations, + in Fig. 5C) that tend to border the holes coexist displaying irregular shapes and sizes. This trimodal morphology is quantified in Table 2 where the depth of the holes (depressions) and the height of the fibers (elevations) are shown.

Understanding all the structures observed is not trivial and would require additional information from other techniques. Anyway, it is possible to interpret the characteristics of the phospholipid/Ca^{2+}/DNA ternary system, considering the size and morphologies of the interfacial structures visualized in Fig. 5. Therefore, the fibers (marked with + in Fig. 5C) possibly correspond to phospholipid/Ca^{2+}/DNA interfacial aggregates considering their dimensions which are clearly greater than one single DNA chain. The removal of phospholipids from the monolayer to form aggregates may explain the appearance of holes (marked with – in Fig. 6A). Finally, the granular domains (marked with * in Fig. 5C) constitute a more complex form of interfacial aggregates. Similar granular interfacial aggregates have also been found by Antipina *et al.* for octadecylamine/DNA LB monolayers.[32] This morphology could be caused by DNA strands covered with phospholipid vesicles formed from the monolayer as a result of the interfacial complexation.

Compression up to 40 mN m^{-1} resulted mainly in an increase in the area of the background as shown in Fig. 6A. The structure in the background of Fig. 6A is very similar to that described at 25 mN m^{-1} (Fig. 5). However, Fig. 6A reveals the existence of regions of irregular shape and size that are significantly thicker than the background. These structures appear only at higher interfacial coverage (40 mN m^{-1}) and were not seen at 25 mN m^{-1} (Fig. 5). Again, the trimodal morphology is quantified in Table 2 where the depth of the holes (depressions) and the height of the fibers (elevations) are shown demonstrating the similarities with lower surface coverage.

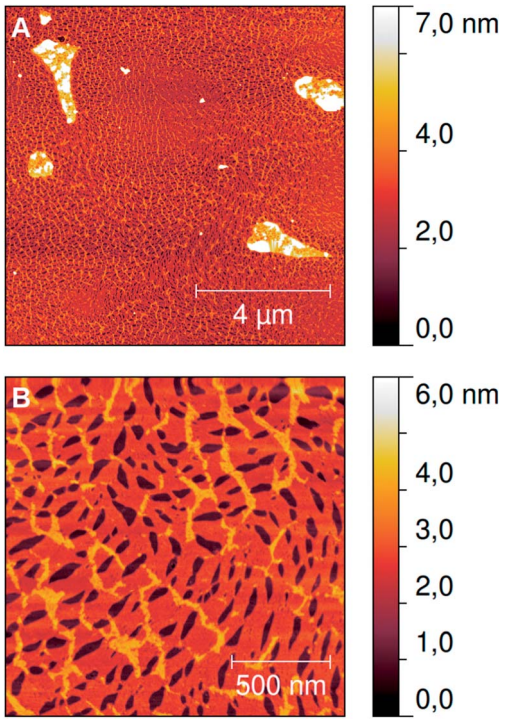

Fig. 6 (A) AFM topography image of LB transferred DPPC/DPPS 4 : 1 spread on an aqueous solution subphase containing 5 mM $CaCl_2$ and 0.1 ctmg ml^{-1} DNA at $\pi = 40$ mN m^{-1}. (B) High resolution image. Images show a background composed of a discontinuous plane spotted by regions significantly thicker of irregular shape and size.

The height distribution profile of the ternary system at higher interfacial coverage (40 mN m^{-1}) is plotted in Fig. 7. This plot shows three peaks corresponding to the three different height levels observed in the ternary system (Fig. 5, 6 and Table 2). Although Fig. 7 shows the values corresponding to the system at 40 mN m^{-1}, this trimodal morphology extends to the ternary system at 25 mN m^{-1} as quantified in Table 2.

Hence, the phospholipid/Ca^{2+}/DNA ternary system forms a background composed of a discontinuous plane spotted with holes (depressions) and fibers (elevations). According to the height distribution profile (Fig. 7), the holes and fibers observed

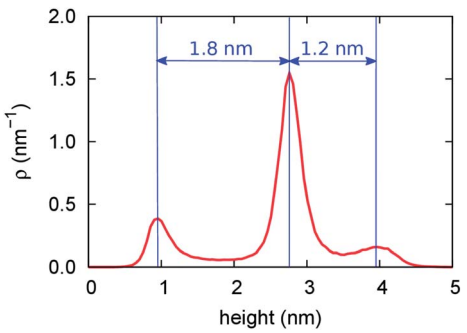

Fig. 7 Height distribution function obtained from the AFM image in Fig. 6B. This curve is representative of the topography obtained at 40 mN m^{-1}.

should be located, on average, at −1.8 nm and 1.2 nm with respect to the most abundant height, respectively. The difference in height between the first and the second peak is 1.8 nm (Fig. 6 and Table 2). The measured heights allow us to identify the morphologies with the composition. This value reasonably matches the thickness of a DPPC LB monolayer on mica reported in the literature:[51] 2.2 nm. Hence, this allows us to conclude from Fig. 5 and 6 that the phospholipid monolayer is discontinuous, being interrupted by the holes. Furthermore, the height of the fibers with respect to the LB phospholipid monolayer according to Table 2 is 1.2 nm (Fig. 7). This value agrees with that reported by Wu *et al.* for the increase in thickness of a lipid/DNA monolayer with respect to the pure lipid monolayer of 0.9 nm.[52] Accordingly, the fibers observed in Fig. 5, 6 and 7 correspond to phospholipid/Ca^{2+}/DNA interfacial aggregates. The height values obtained from our AFM images mostly agree with those reported in the literature[51,52] for the LB monolayer thickness of lipid and lipid/DNA. Slight differences encountered could be due to the different system used and also to the surface–tip interactions in AFM (tapping mode), which are expected to change when the tip is scanning the different parts or domains in these complex LB monolayers. Therefore, the topographical profile given in Fig. 7 illustrates the complexation of negatively charged phospholipid monolayers and DNA mediated by Ca^{2+}.

A plausible multifunctional scenario can be hypothesized for the complexation of DNA with anionic lipid monolayers. Depending on the lateral packing as quantified by the surface pressure, the lipid/DNA complex can be expected to undergo various conformational transitions. Moreover, the complexation results in the formation of interfacial aggregates that show a variety of morphologies depending on such lateral packing. The proposed methodological approach combining AFM with monolayers can be productively exploited as a generic tool to explore the molecular mechanism underlying the complexation of DNA with negatively charged lipids toward the rational design of biocompatible systems.

4. Conclusions

The complexation of anionic phospholipid DPPC/DPPS 4 : 1 monolayers and negatively charged DNA in Langmuir monolayers is mediated by Ca^{2+}. Such complexation is confirmed by a shift to higher molecular areas in the π–A isotherm recorded only for the ternary system (phospholipid/Ca^{2+}/DNA). The DNA is expelled from the monolayer at high lateral compression and the surface pressure modulates the complexation at the interface. Gibbs elasticity provides evidence for a fluidisation of the system owing to the complexation and reveals a whole new phase transition map of the monolayer. AFM imaging allows visualization of the complexation at the interface which gives rise to the formation of interfacial aggregates, whose morphology and size again depend on the lateral packing and hence could be potentially modulated by the surface pressure. At low surface pressures, DNA complexes mainly at DPPS-enriched domains forming fractal, net-like structures. At higher surface pressure, the lipid/DNA complexation leads to the

formation of fibers lying on a discontinuous monolayer. From these results, we visualise the complexation for the first time and more importantly we can rationally control the binding of DNA to anionic lipid monolayers by modulating the surface pressure of the system.

Acknowledgements

The authors thank the financial support from the following projects: (i) PERG07-GA-2010-268315-ColloDi from European Union-FP7, (ii) RyC-2012-10556, MAT2010-20370, MAT2011-23339, MAT2012-36270-C04-04 and -02, from MICINN and MINECO, (iii) P08-FQM-4325 and P09-FQM-4698 from 'Consejería de Innovación, Ciencia y Empresa de la Junta de Andalucía' and (iv) CEI2013-MP-3 from 'Campus de Excelencia Internacional (CEI BioTic)-Universidad de Granada'.

Notes and references

1 C. T. de Ilarduya, Y. Sun and N. Duezguenes, *Eur. J. Pharm. Sci.*, 2010, **40**, 159–170.
2 A. Schroeder, C. G. Levins, C. Cortez, R. Langer and D. G. Anderson, *J. Intern. Med.*, 2010, **267**, 9–21.
3 D. Pozzi, G. Caracciolo, R. Caminiti, S. C. De Sanctis, H. Amenitsch, C. Marchini, M. Montani and A. Amici, *ACS Appl. Mater. Interfaces*, 2009, **1**, 2237–2249.
4 I. Koltover, T. Salditt, J. O. Radler and C. R. Safinya, *Science*, 1998, **281**, 78–81.
5 J. O. Radler, I. Koltover, T. Salditt and C. R. Safinya, *Science*, 1997, **275**, 810–814.
6 M. Muñoz-Ubeda, A. Rodriguez-Pulido, A. Nogales, O. Llorca, M. Quesada-Perez, A. Martin-Molina, E. Aicart and E. Junquera, *Soft Matter*, 2011, **7**, 5991–6004.
7 M. Muñoz-Ubeda, A. Rodriguez-Pulido, A. Nogales, A. Martin-Molina, E. Aicart and E. Junquera, *Biomacromolecules*, 2010, **11**, 3332–3340.
8 A. L. Barran-Berdon, M. Muñoz-Ubeda, C. Aicart-Ramos, L. Perez, M. R. Infante, P. Castro-Hartmann, A. Martin-Molina, E. Aicart and E. Junquera, *Soft Matter*, 2012, **8**, 7368–7380.
9 D. Paiva, A. Martin-Molina, I. Cardoso, M. Quesada-Perez, M. D. Pereira and S. Rocha, *Soft Matter*, 2013, **9**, 401–409.
10 S. D. Patil, D. G. Rhodes and D. J. Burgess, *AAPS J.*, 2004, **6**, e29.
11 S. D. Patil, D. G. Rhodes and D. J. Burgess, *Biochim. Biophys. Acta, Biomembr.*, 2005, **1711**, 1–11.
12 A. Martín-Molina, G. Luque-Caballero, J. Faraudo, M. Quesada-Pérez and J. Maldonado-Valderrama, *Adv. Colloid Interface Sci.*, DOI: 10.1016/j.cis.2013.11.005.
13 C. Srinivasan and D. J. Burgess, *J. Controlled Release*, 2009, **136**, 62–70.
14 H. J. Liang, D. Harries and G. C. L. Wong, *Proc. Natl. Acad. Sci. U. S. A.*, 2005, **102**, 11173–11178.
15 M. R. Mozafari, C. J. Reed, C. Rostron and V. Hasirci, *J. Liposome Res.*, 2005, **15**, 93–107.
16 A. Rodriguez-Pulido, A. Martin-Molina, C. Rodriguez-Beas, O. Llorca, E. Aicart and E. Junquera, *J. Phys. Chem. B*, 2009, **113**, 15648–15661.
17 S. Ohki and N. Duzgunes, *Biochim. Biophys. Acta*, 1979, **552**, 438–449.
18 S. Roldan-Vargas, A. Martin-Molina, M. Quesada-Perez, R. Barnadas-Rodriguez, J. Estelrich and J. Callejas-Fernandez, *Phys. Rev. E: Stat., Nonlinear, Soft Matter Phys.*, 2007, **75**, 021912.
19 S. Roldan-Vargas, R. Barnadas-Rodriguez, A. Martin-Molina, M. Quesada-Perez, J. Estelrich and J. Callejas-Fernandez, *Phys. Rev. E: Stat., Nonlinear, Soft Matter Phys.*, 2008, **78**, 010902.
20 A. Martin-Molina, C. Rodriguez-Beas and J. Faraudo, *Biophys. J.*, 2012, **102**, 2095–2103.
21 L. A. Wangerek, H. H. M. Dahl, T. J. Senden, J. B. Carlin, D. A. Jans, D. E. Dunstan, P. A. Ioannou, R. Williamson and S. M. Forrest, *J. Gene Med.*, 2001, **3**, 72–81.
22 R. Marty, C. N. N'soukpoe-Kossi, D. Charbonneau, C. M. Weinert, L. Kreplak and H. A. Tajmir-Riahi, *Nucleic Acids Res.*, 2009, **37**, 849–857.
23 J. H. Kim, S. Y. Yim, M. K. Oh, M. D. Phan and K. Shin, *Soft Matter*, 2012, **8**, 6504–6511.
24 G. Thakur, C. Pao, M. Micic, S. Johnson and R. M. Leblanc, *Colloids Surf., B*, 2011, **87**, 369–377.
25 S. Kundu, H. Matsuoka and H. Seto, *Colloids Surf., B*, 2012, **93**, 215–218.
26 M. Dittrich, M. Bottcher, J. S. L. Oliveira, B. Dobner, H. Mohwald and G. Brezesinski, *Soft Matter*, 2011, **7**, 10162–10173.
27 R. C. MacDonald, A. Gorbonos, M. M. Mornsen and H. L. Brockman, *Langmuir*, 2006, **22**, 2770–2779.
28 D. McLoughlin, R. Dias, B. Lindman, M. Cardenas, T. Nylander, K. Dawson, M. Miguel and D. Langevin, *Langmuir*, 2005, **21**, 1900–1907.
29 L. Cristofolini, T. Berzina, S. Erokhina, O. Konovalov and V. Erokhin, *Biomacromolecules*, 2007, **8**, 2270–2275.
30 A. Frantescu, K. Tonsing and E. Neumann, *Bioelectrochemistry*, 2006, **68**, 158–170.
31 J. Maldonado-Valderrama, A. P. Gunning, P. J. Wilde and V. J. Morris, *Soft Matter*, 2010, **6**, 4908–4915.
32 M. N. Antipina, R. V. Gainutdinov, A. A. Rachnyanskaya, A. L. Tolstikhina, T. V. Yurova and G. B. Khomutov, *Surf. Sci.*, 2003, **532–535**, 1025–1033.
33 Q. Chen, X. Kang, R. Li, X. Du, Y. Shang, H. Liu and Y. Hu, *Langmuir*, 2012, **28**, 3429–3438.
34 X. D. Chen, L. Li and M. H. Liu, *Langmuir*, 2002, **18**, 4449–4454.
35 E. V. Dubrovin, S. N. Staritsyn, S. A. Yakovenko and I. V. Yaminsky, *Biomacromolecules*, 2007, **8**, 2258–2261.
36 M. Ross, C. Steinem, H. J. Galla and A. Janshoff, *Langmuir*, 2001, **17**, 2437–2445.
37 M. Larguinho, H. M. Santos, G. Doria, H. Scholz, P. V. Baptista and J. L. Capelo, *Talanta*, 2010, **81**, 881–886.
38 S. Kundu, D. Langevin and L. T. Lee, *Langmuir*, 2008, **24**, 12347–12353.
39 F. Behroozi, *Langmuir*, 1996, **12**, 2289–2291.

40 V. J. Morris and A. P. Gunning, *Soft Matter*, 2008, **4**, 943–951.
41 G. Ma and H. C. Allen, *Langmuir*, 2006, **22**, 5341–5349.
42 S. Gromelski and G. Brezesinski, *Phys. Chem. Chem. Phys.*, 2004, **6**, 5556.
43 D. H. Mengistu, K. Bohinc and S. May, *J. Phys. Chem. B*, 2009, **113**, 12277–12282.
44 S. Gromelski and G. Brezesinski, *Langmuir*, 2006, **22**, 6293–6301.
45 X. M. Li, J. M. Smaby, M. M. Momsen, H. L. Brockman and R. E. Brown, *Biophys. J.*, 2000, **78**, 1921–1931.
46 N. J. Jain, P. A. Albouy and D. Langevin, *Langmuir*, 2003, **19**, 5680–5690.
47 C. G. Sinn, M. Antonietti and R. Dimova, *Colloids Surf., A*, 2006, **282**, 410–419.
48 R. A. Dluhy, D. G. Cameron, H. H. Mantsch and R. Mendelsohn, *Biochemistry*, 1983, **22**, 6318–6325.
49 A. Martin-Molina, C. Rodriguez-Beas and J. Faraudo, *Phys. Rev. Lett.*, 2010, **104**, 168103.
50 J. Faraudo and A. Martin-Molina, *Curr. Opin. Colloid Interface Sci.*, 2013, **18**, 517–523.
51 K. Kim, C. Kim and Y. Byun, *Langmuir*, 2001, **17**, 5066–5070.
52 J. C. Wu, T. L. Lin, U. S. Jeng and N. Torikai, *Phys. B*, 2006, **385-86**, 838–840.